ACS APPLIED MATERIALS & INTERFACES

Research Article

www.acsami.org

Self-Assembly of Diblock Polythiophenes with Discotic Liquid Crystals on Side Chains for the Formation of a Highly Ordered Nanowire Morphology

Xun Chen,[†] Lie Chen,[†,‡] Kai Yao,[†] and Yiwang Chen*[,†,‡]

[†]Institute of Polymers/Department of Chemistry, Nanchang University, 999 Xuefu Avenue, Nanchang 330031, China

[‡]Jiangxi Provincial Key Laboratory of New Energy Chemistry, Nanchang University, 999 Xuefu Avenue, Nanchang 330031, China

Supporting Information

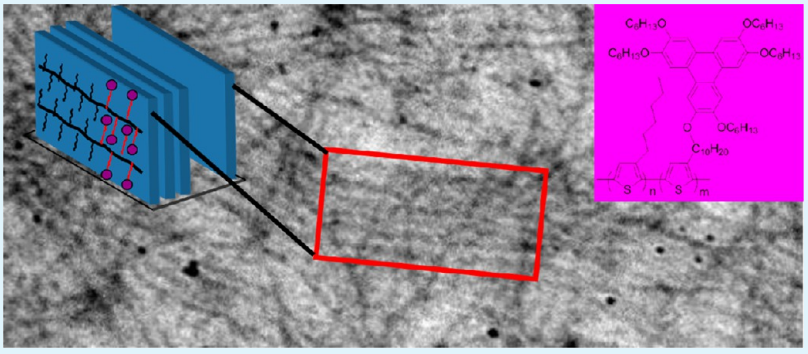

ABSTRACT: Diblock copolymers bearing a triphenylene (TP) discotic liquid crystals moiety, poly(3-hexylthiophene)-block-poly[3-(10-(2,3,6,7,10-pentakis(hexyloxy)triphenylen)-decyloxy)thiophene] (P3HT-b-P3TPT), was successfully synthesized by Grignard metathesis polymerization. The self-assembled nanowire structures of these diblock copolymers have been investigated by atomic force microscopy and transmission electron microscopy. The domain size and crystallinity of the nanostructures can be easily controlled by tuning the P3HT/P3TPT block ratio and by employing different annealing processes such as thermal and solvent annealing. The results of X-ray diffraction indicate that both intermolecular interactions and mesogen packing are essential for the formation of nanostructures in the diblock copolymers. Although the block ratio of P3HT and P3TPT comes to 9:1 and the copolymer undergoes solvent annealing followed by thermal treatment, an optimal crystalline nanowire with a size of 16.9 nm is formed. In addition, solar cells based on these copolymers as electron donors in combination with [6,6]-phenyl-C_{61}-butyric acid methyl ester ($PC_{61}BM$) or *N*,*N*′-di(2-ethylhexyl)perylene-3,4,9,10-tetracarboxylbisimide (PDI) as electron acceptors have been constructed, and the effect of the nanomorphology on device performance has been investigated.

KEYWORDS: *liquid crystals, block polymers, conjugated polymers, self-assembly, fullerene, polymer solar cells*

INTRODUCTION

It has been reported that the efficiency of bulk-heterojunction (BHJ) organic solar cells heavily depends on the precise control of the nanoscale morphology of the active layer because the lifetime of the exciton is short, and its exciton diffusion length is much smaller than the optical absorption length in organic materials.[1−5] Among several strategies, the self-assembly of block copolymers can provide an effective opportunity for developing the well-ordered nanoscale morphology.[6,7] Intermolecular and intramolecular interactions between the dissimilar blocks enable the polymer chains to self-assemble into a series of nanostructures with controllable dimensions and functionalities. A large variety of nanoscale structures, such as fibrillar, lamellar, and sphere structures, are observed in the block copolymers, as reported by Russell's group.[8−10] These ordered nanoscale architectures built by block copolymers offer an effective approach to tune the morphology of the active layer, which can meet the requirement for different organic photovoltaic devices.[11,12]

One of the most common polymers extensively studied in BHJ solar cells is regioregular poly(3-hexylthiophene) (P3HT) because of its high charge carrier mobility and improved spectral sensitivity in the light aborption.[13−15] Considerable efforts to control the nanoscale arrangement of P3HT chains have been conducted by process optimization, including thermal annealing,[16,17] solvent annealing,[18−21] and the use of an additive.[22] Thus, by combining the advantages of these process optimizations with the self-assembly property of block copolymers, the synthesis and morphology of P3HT-based block copolymers have been extensively studied by McCullough's group.[23−25] For example, compared to P3HT

Received: January 8, 2013
Accepted: August 6, 2013
Published: August 6, 2013

Scheme 1. Synthesis of Diblock Copolymers P3HT-b-P3TPT[a]

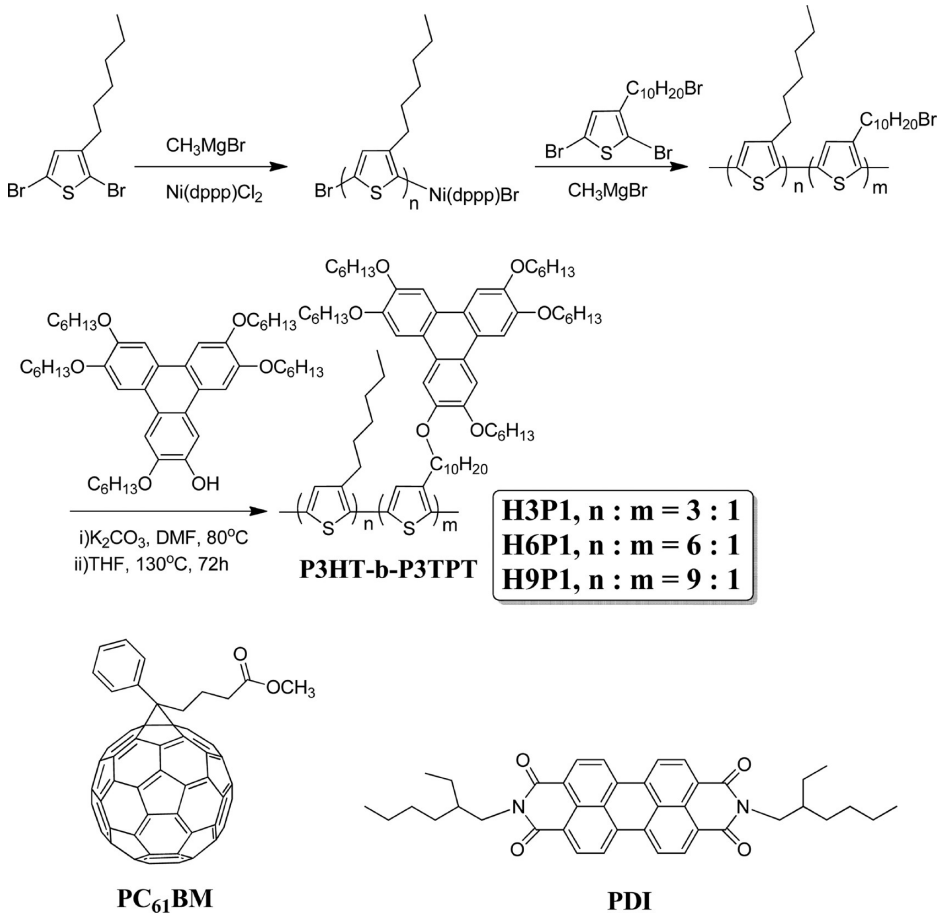

[a][6,6]-phenyl-C_{61}-butyric acid methyl ester ($PC_{61}BM$) and *N,N′*-di(2-ethylhexyl)perylene-3,4,9,10-tetra-carboxylbisimide (PDI) as electron acceptors have been discussed in bulk heterojunction solar cells.

homopolymer, the P3HT-based rodlike diblock copolymers can achieve more ordered lamellar nanostructures and fascinating electronic activity by controlling the proportions of two dissimilar blocks. As such, the effective control over the formation of their desired nanostructures provides attractive opportunities for developing high-performance BHJ solar cells. However, the self-assembly behaviors and physical properties of these rodlike diblock copolymers are far less understood than those of the intensively studied coil-like diblock copolymers, primarily because of the rigid rodlike polymer chains that limits the synthesis and their self-assembly.[26]

Discotic liquid crystals (DLCs), such as triphenylene, are particularly attractive for various device applications because the 1D columnar structure, resulting from strong intermolecular interactions between the planar aromatic cores, has been regarded as an efficient pathway for charge transport along the columnar axis.[27,28] However, its application in the field of BHJ organic solar cells has not been widely studied. This situation inspired us to design a rod−rod diblock copolymer with liquid-crystalline nature to improve and optimize the crystalline nanostructure by spontaneous phase separation.

In this Article, we reported the synthesis of diblock copolymers bearing a triphenylene liquid-crystalline pendant, poly(3-hexylthiophene)-block-poly[3-(10-(2,3,6,7,10-pentakis-(hexyloxy)triphenylen)decyloxy)thiophene] (P3HT-b-P3TPT). The self-assembled morphology of these P3HT-b-P3TPT diblock copolymers is investigated by atomic force microscopy (AFM), transmission electron microscopy (TEM), and X-ray diffraction (XRD). We found that fusing a diblock structure with liquid-crystalline nature could enable these copolymers to form an extremely well-defined nanowire with 10−20 nm crystalline size, which is beneficial for charge transport. Moreover, these block copolymers are further used in BHJ solar cells with two different kinds of electron acceptors ($PC_{61}BM$ and PDI), and the effect of their BHJ morphology on device performance has been studied.

RESULTS AND DISCUSSION

The unsymmetrical monohydroxytriphenylene derivative, namely, 3,6,7,10,11-penta(hexyloxy)-2-hydroxytriphenylene (TP), was synthesized according to the procedure reported in the literature.[29] The targeted diblock copolymers, P3HT-b-P3TPT, were synthesized as described in Scheme 1. (Also, see the Supporting Information.) The first P3HT block was synthesized through Grignard metathesis polymerization of 2,5-dibromo-3-hexylthiophene to obtain a polymer with a living chain end, which was chain extended into the diblock structure by adding alkyl-bromide-substituted thiophene monomer. The bromine units in the resulting P3HT-b-P3BrDT diblock polymers were replaced with TP groups through a Williamson ether reaction to yield targeted diblock copolymers P3HT-b-P3TPT. The complete conversion of bromine atoms to TP groups in these copolymers was confirmed by ^{1}H NMR (Figure 1), where the signal of methylene (adjacent to bromine atom)

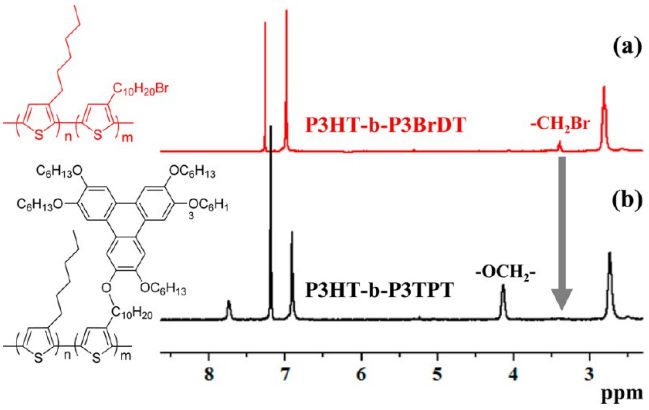

Figure 1. ^{1}H NMR spectra of (a) P3HT-b-P3BrDT and (b) P3HT-b-P3TPT after complete substitution by the triphenylene derivatives.

shifted from 3.40 to 4.10 ppm, which is assigned to the methylene group adjacent to the oxygen atom. These diblock copolymers were designed with P3HT as the major block to improve crystallinity and to offer the reactive functionality to perform chemistry on the self-assembled structures.[30] Three diblock copolymers were systematically investigated here, having P3HT/P3TPT molar ratios of 3:1, 6:1, and 9:1, termed H3P1, H6P1, and H9P1, respectively. The actual block ratios in the copolymers were measured from the integral ratio between the signal at 4.10 ppm (assigned to methylene group adjacent to the oxygen atom) and the signal at 2.80 ppm (assigned to methylene group adjacent to the thiophene ring). The measured compositions in these copolymers are very close to the feed ratios (75:25, 85:15, and 90:10) of the monomers. The molecular weights were estimated by gel permeation chromatography (GPC) using tetrahydrofuran as the eluent.

Polarized-light optical microscopy (POM) image shows that the monomer TP exhibits the conic fan-type texture when cooling from the isotropic state, as depicted in Figure 2a, which is a typical feature of the columnar phase. The XRD pattern of TP at 81 °C (Figure 2b) reveals diffraction peaks at 16.3, 9.4, and 8.2 Å in the low-angle regions, where the *d*-spacing values ratio is $1:1/3^{1/2}:1/_2$, which is attributed to the (100), (110), and (200) diffraction of the hexagonal columnar (Col_h) phase, respectively.[31] In addition, the obvious diffraction peak appears at 3.45 Å, which is associated with the typical $\pi-\pi$ stacking in the individual column. The thermal behavior of triphenylene-functionalized diblock copolymers P3HT-b-P3TPT was also investigated by POM and DSC. Under POM, these copolymers do not display obvious optical textures. Thus, it is not possible to test the liquid-crystalline phase. However, for the H3P1 and H6P1 copolymers, a birefringent texture is observed from room temperature to about 130 °C, indicating a liquid-crystalline property. However, H9P1 hardly shows any bright texture during the heating process because of the lower content of triphenylene discs. DSC analysis agrees well with the POM obervation (Figure S7). Although only one endothermic peak appears in second heating scan of each copolymer, with the aid of POM, the endothermic peak at 127 °C for H3P1 and at 139 °C for H6P1 is identified as the transition from the liquid-crystalline state to the isotropic state. Therefore, the phase transition behaviors of P3HT-P3TPT copolymers have been significantly influenced by the liquid-crystalline property of the triphenylene group.[32]

UV−vis absorption spectra of the copolymer films via different treatments such as as-cast, thermal annealing (TA), and *ortho*-dichlorobenzene (*o*-DCB) vapor annealing followed by thermal annealing (SA + TA) are shown in Figure 3. (See the Supporting Information for details). From Figure 3a−c, we can see that the absorption spectra of H9P1, H6P1, and H3P1 thin solid films are basically the same, showing two characteristic absorption peaks. The peak in the ultraviolet region (280 nm) can be assigned to the $\pi-\pi$ transition of TP groups,[33] whereas the band in the visible-light region (510−610 nm) results from the absorption of the P3HT backbone. The absorption spectra of TP monomer and P3HT homopolymer were also presented as references in Figure 3. The solid-state absorption spectra of these block copolymers in the visible-light region are essentially similar to that of P3HT homopolymer, exhibiting absorption maxima at 540−560 nm with two shoulders at 510−520 and 600−610 nm. The shoulder at 603 nm for P3HT-b-P3TPT results from the formation of highly ordered lamellar structures[34] despite the existence of the P3TPT block. Surprisingly, direct thermal annealing (TA) exerts little effect on the absorption bands of both copolymers. However, if we conducted solvent annealing before thermal annealing, it (SA + TA) leads to a relatively higher intensity of the absorption shoulder peak (603 nm) for H9P1 and H6P1 than that of the direct thermal treatment. This suggests that the slow film growth can assist the formation of a self-organized ordered structure resulting from diminished intermolecular

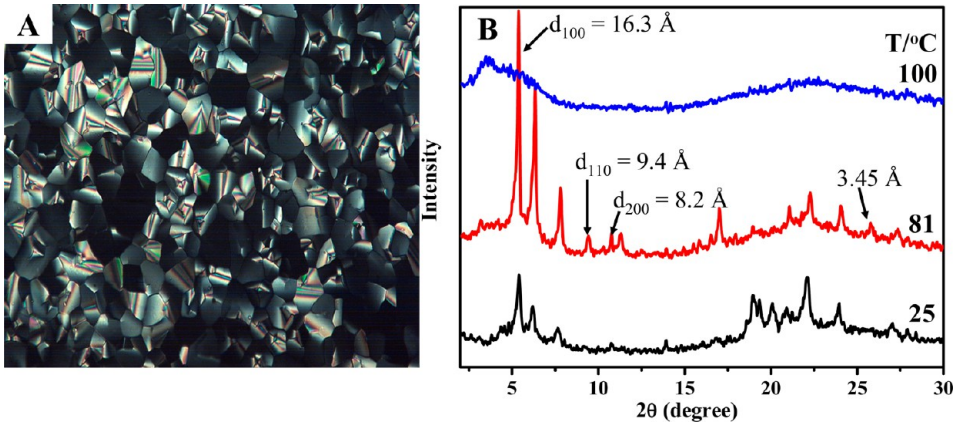

Figure 2. (a) POM image of monomer TP obtained on cooling to 81 °C from the isotropic phase. (a) XRD profiles of monomer TP obtained at 25 (solid phase), 81 (liquid-crystalline phase), and 100 °C (isotropic phase).

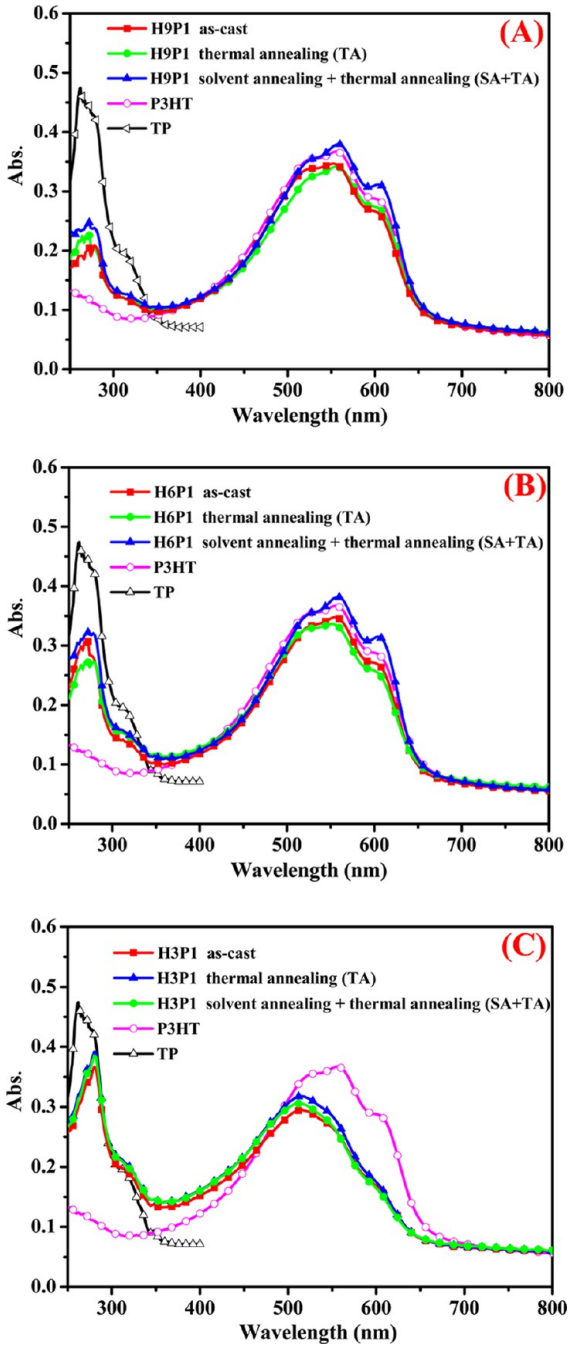

Figure 3. UV–vis spectra of the thin films of (a) H9P1, (b) H6P1, and (c) H3P1 under different treatments in comparison with the spectra of TP and P3HT.

coupling.[21] The subsequent thermal treatment strengthens their crystallinity with the help of the supramolecular organizations of the TP discs.[35] However, for the direct TA treatment, the original arrangement of polymer chains and discotic mesogens in the copolymer films is not favorable for developing well-organized nanostructures under fast film growth conditions. Therefore, the optical spectra of P3HT-b-P3TPT indicate that combining slow film growth (SA) with mesogen orientation under TA conditions is very helpful for the self-assembly of diblock copolymers into a more highly ordered nanoscale morphology. However, the H3P1 copolymer film, whether annealed or not, shows a notable blue shift with respect to the P3HT homopolymer. This is because the presence of too many disc substituents appears to disturb the $\pi-\pi$ stacking of the polythiophene.

The packing and orientation of the polymer chains in the P3HT-b-P3TPT thin films were studied further by XRD. Figure 4a shows the XRD patterns of the annealed H9P1, H6P1, and

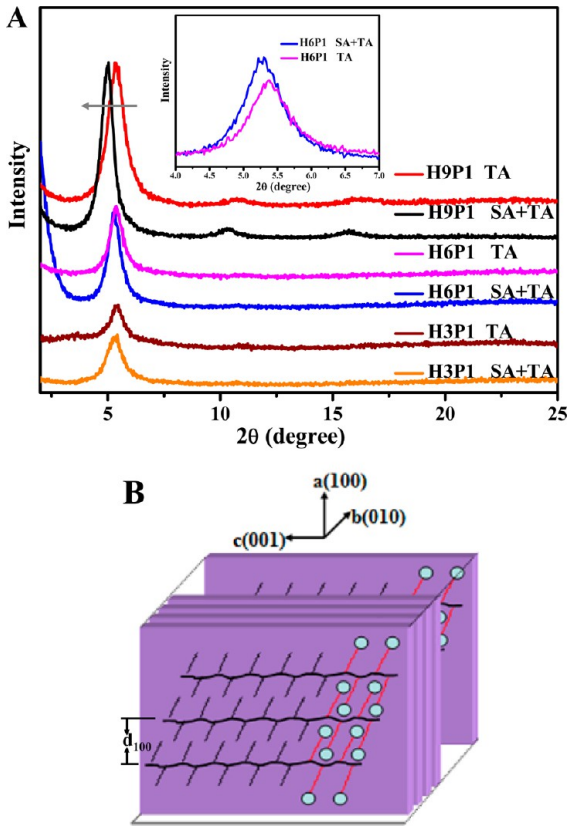

Figure 4. (a) XRD profiles of the H9P1, H6P1, and H3P1 films treated with TA and with SA + TA. (b) Schematic representation of P3HT-b-P3TPT (H9P1, H6P1, and H3P1) lamella packing with the edge-on orientation.

H3P1 films prepared from *o*-DCB solutions, all of which show a strong (100) diffraction peak at $2\theta = 5.3°$, corresponding to the inter-P3HT *d*-spacing of the alkyl side chain.[36] This indicates that the P3HT-b-P3TPT copolymers still adopt the edge-on orientation, where the $\pi-\pi$ interchain stacking of the thiophene backbone is parallel to the silicon wafer, whereas the alkyl side chains of the P3HT block are oriented vertically with respect to the substrate.[37] The schematic illustration of the molecular arrangement in the P3HT-b-P3TPT copolymers is depicted in Figure 4b. Intriguingly, the diffraction peak that emerged in the H6P1 film is slightly shifted to the lower-angle region under SA + TA treatment in comparison with that of the TA treatment. The domain size and *d*-spacing value are calculated from the information on the (100) diffraction peak by the Scherrer's and Bragg's equations,[38] respectively. From Table S1, we can see that the domain size and *d*-spacing are higher for the SA + TA treated film than for that of the TA treated film. This suggests that the SA pretreatment prolongs the film growth and helps the molecules to form a relatively ordered lamellar structure. In fact, the self-assembly microstructure is correlated with the packing competition between the interchain interactions and mesogen orientation. Although the orientation of the triphenylene discs facilitates the molecular arrangement in the

dx.doi.org/10.1021/am402031v | ACS Appl. Mater. Interfaces 2013, 5, 8321–8328

polymers, too many discs tend to disrupt the polythiophene interchain interaction even after long solvent-annealing times. Evidently, polymer H3P1, with a high disc content, sterically hinders the crystalline growth of polymer backbones under both direct TA and SA + TA treatments, as evidenced by the weak and broad peaks of H3P1. Moreover, the shift to a lower-angle region is more distinct for copolymer H9P1 that has a lower DLC content, indicating a more ordered lamellar-stacking orientation. In addition, for the (100) reflection of the H9P1 films, the crystallite size is 13.2 nm for the TA treatment and 16.9 nm for SA + TA treatment, which is consistent with that estimated by TEM (discussed later). Therefore, an appropriate amount of DLC is essential to molecular packing.

The improved morphology of H6P1 and H9P1 is supported by AFM analysis. Figure 5 shows the topographic and phase

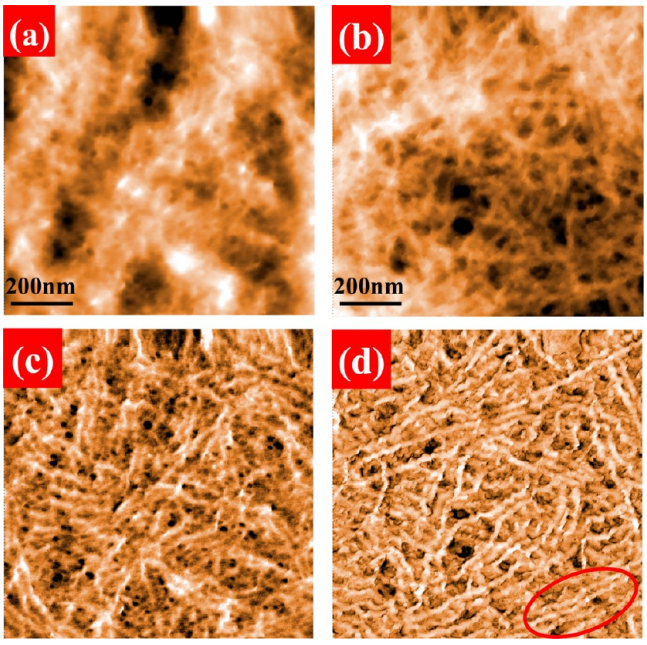

Figure 5. AFM images of spin-coated polymers. (a) Topographic and (c) phase images of H6P1 films with SA + TA treatment; (b) topographic and (d) phase images of H9P1 films with SA + TA treatment.

AFM images of the H6P1 and H9P1 films. From the phase images of the SA + TA treated P3HT-b-P3TPT films, some bright and dark regions with distinct boundaries are observed, suggestive of different rigidities within these nanoscale domains. Both nanoscale domains form a continuously ordered lamellar structure driven by the crystalline nature of the P3HT domains. Clearly, a more densely interconnected nanowire structure is exhibited in the H9P1 film because of its higher degree of crystallization, and its nanowire length is extended over hundreds of nanometers. In sharp contrast, as the block content of P3TPT increases, H6P1 self-assembles to form only short and less-dense nanowires. These results clearly indicate that these nanostructures can be attributed to the interplay between the self-assembly and phase separation of the P3HT and P3TPT blocks, and the size of nanostructures depends on the relative ratio of the P3HT and P3TPT blocks. However, for the direct thermal treated or direct solvent treated H9P1 film, the AFM images (Figure S8) show a rough surface without nanowire structures. In addition, the SA + TA treated P3HT film does not show a similar nanostructure morphology (Figure S8). It indicates that both the well-organized diblock copolymers under slow film growth and the mesogen orientation under TA conditions are very important for the formation of the nanostructure. SA + TA treatment can also reduce the interruption of the liquid-crystalline self-assembly on the chain interactions. However, increasing the content of the P3TPT block to 1:4 (H3P1) greatly enables the discs to take advantage of the competition between the interchain interactions and mesogen orientation, which totally disrupts the self-assembly of the polythiophene chains and results in a less-ordered nanostructure (Figure S8).

Furthermore, the ordered morphology of these diblock copolymers was also demonstrated by TEM. From the TEM images in Figure 6, we can see that the self-assembly nanowires

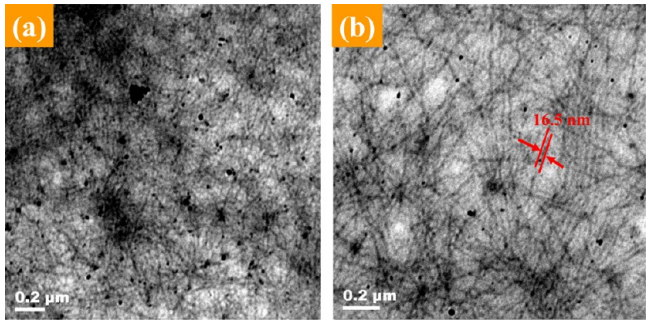

Figure 6. TEM images of the nanowires assembled from diblock copolymers (a) H6P1 and (b) H9P1 films prepared by SA + TA treatment.

in the P3HT-b-P3TPT films are similar to the results observed in the AFM images. Figure 6b shows that the SA + TA treated H9P1 film tends to form highly well-organized nanowires with an average diameter of ~17 nm. Such a 1D nanowire structure may provide a desirable pathway for efficient charge transport. At the same time, the nanomorphology composed of regular parallel-striped domains with a lamellar nanostructure can be observed. As expected, the H6P1 film only shows a poor network structure with less-ordered and smaller diameter (~12.6 nm) wires (Figure 6a).

The photovoltaic application of these block copolymers was performed by blending them with various electron acceptors. Figure 7 shows the typical current density–voltage (J–V) curves of the P3HT-b-P3TPT/$PC_{61}BM$ devices, and the performance data of the devices (PCE, V_{OC}, J_{SC}, and FF) are listed in Table 1. The bulk heterojunction device based on the SA + TA treated H9P1/$PC_{61}BM$ blend exhibits the best performance with a PCE of 1.54%, J_{SC} of 6.51 mA/cm^2, V_{OC} of 0.601 V, and FF of 0.394, whereas the device based on its analogous block copolymers H6P1 and H3P1 only shows PCE values of 0.99 and 0.24%, respectively. A reference solar cell constructed with an optimized P3HT/$PC_{61}BM$ device shows a PCE value of 2.78%, with a J_{SC} of 7.35 mA/cm^2, V_{OC} of 0.655 mV, and FF of 0.578. The performance parameters imply that the devices based on P3HT-b-P3TPT possess lower J_{SC} and FF than the device based on P3HT/$PC_{61}BM$, resulting in the decreased device performance. The lower J_{SC} of the P3HT-b-P3TPT/$PC_{61}BM$ devices may be related to the large phase-separation morphology of the active layer, resulting from the reduced compatibility between the bulky pendant triphenylene moieties and $PC_{61}BM$. However, for direct TA treatment, H3P1, H6P1, and H9P1 show poor performance, with PCE

dx.doi.org/10.1021/am402031v | ACS Appl. Mater. Interfaces 2013, 5, 8321–8328

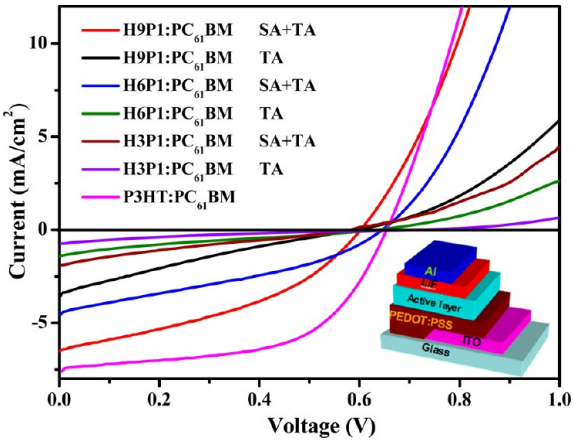

Figure 7. *J*–V characteristics of photovoltaic cells based on H9P1/$PC_{61}BM$, H6P1/$PC_{61}BM$, and H3P1/$PC_{61}BM$ (1:2 w/w), with P3HT/$PC_{61}BM$ (1:1 w/w) as a reference under AM 1.5G illumination.

Table 1. Solar Cell Performance Parameters of P3HT/$PC_{61}BM$, H9P1/$PC_{61}BM$, H6P1/$PC_{61}BM$, and H3P1/$PC_{61}BM$ Blends after TA or SA + TA Treatments

components	V_{OC} (V)	J_{SC} (mA/cm^2)	*FF*	PCE (%)
H9P1/$PC_{61}BM^a$ (1:2)[d]	0.601	6.51	0.394	1.54
H9P1/$PC_{61}BM^b$ (1:2)	0.587	3.61	0.207	0.44
H6P1/$PC_{61}BM^a$ (1:2)	0.648	4.50	0.341	0.99
H6P1/$PC_{61}BM^b$ (1:2)	0.631	1.42	0.202	0.18
H3P1/$PC_{61}BM^a$ (1:2)	0.575	2.09	0.203	0.24
H3P1/$PC_{61}BM^b$ (1:2)	0.693	0.81	0.148	0.08
P3HT/$PC_{61}BM^c$ (1:1)	0.655	7.35	0.578	2.78

[a]SA + TA treatment. [b]TA treatment. [c]Thermally annealed at 150 °C for 10 min. [d]The copolymer/$PC_{61}BM$ device fabricated with a 1:2 w/w shows the best result for each diblock copolymer.

values of 0.08, 0.18, and 0.44%, respectively. The significant decrease in the PCE can be ascribed to the large-scale phase separation and the reduced crystallinity of P3HT-b-P3TPT in the blended films under direct TA treatment. The large phase separation between copolymers and $PC_{61}BM$ is revealed by the XRD analysis (Figure 8) and AFM images (Figure 9) of the active-layer films. Direct TA treatment suppresses the

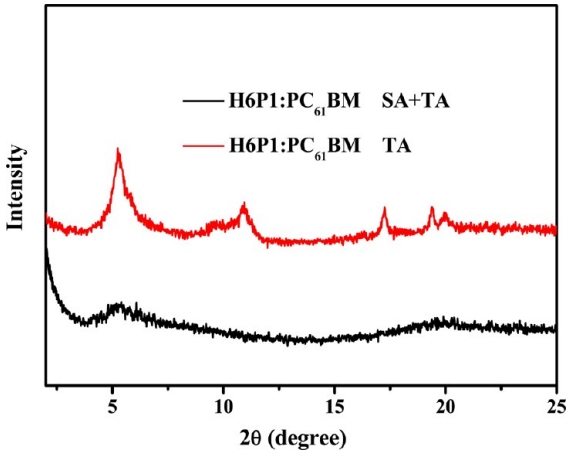

Figure 8. XRD profiles of the films with H6P1/$PC_{61}BM$ blends with TA or SA + TA treatments.

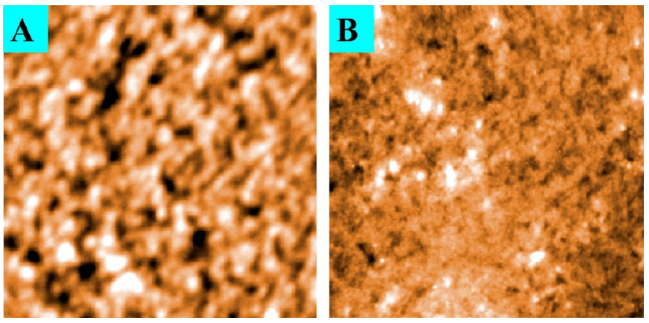

Figure 9. AFM topographic images of H6P1/$PC_{61}BM$ (1:2 w/w) films with (a) direct TA and (b) SA + TA treatments. The image size is 5 × 5 um^2.

interchain interactions of P3HT and leads to the amorphous domains of polythiophene. On the contrary, the SA + TA treatment can easily drive interchain $\pi-\pi$ interactions to develop the fine formation of crystalline aggregation.

Another DLC member, perylene tetracarboxydiimide (PDI), has been widely studied in BHJ solar cells because of its improved light absorption in the visible range (Figure S9) and higher electron mobility with respect to $PC_{61}BM$.[39] However, solar cells based on blends of PDI and P3HT exhibit only a poor PCE of about 0.2%.[40] This is probably due to the unfavorable morphology for charge transport, originating from the formation of micrometer-sized PDI aggregates. An improvement in PCE has been realized using a DLC-functionalized copolymer as a compatibilizer in Frechet groups.[41] The molecular interaction between the two discotic materials produced an ordered morphology.

To tune the desirable miscibility of the donor and acceptor, a similar discotic liquid-crystal acceptor, PDI, was selected to replace PCBM. By varying the annealing conditions and weight ratios of the active-layer components, the SA + TA treated blend (H6P1/PDI) with a weight ratio of 1:3 yields the best performance of 0.30%, as shown in Table 2. However, the

Table 2. Solar Cell Performance Parameters of the H9P1/PDI, H6P1/PDI, H3P1/PDI, and P3HT/PDI Blends (1:3 w/w) after SA + TA Treatments

components	V_{OC} (V)	J_{SC} (mA/cm^2)	*FF*	PCE (%)
H9P1/PDI	0.544	1.31	0.305	0.21
H6P1/PDI	0.553	1.64	0.331	0.30
H3P1/PDI	0.518	0.40	0.264	0.05
P3HT/PDI	0.530	1.01	0.303	0.16

P3HT/PDI device obtains only a maximum efficiency of 0.16% under the same condition. The increase in PCE is primarily due to the improved J_{SC} (Figure 10), perhaps resulting from optimized nanomorphology. To clarify this, both AFM and TEM were used to study the morphology of these blend films (Figure 11). The AFM and TEM images show that the P3HT/PDI blend presents a severe phase segregation on the micrometer scale with large PDI crystals, as reported in the literature.[42] In contrast, such a large phase separation is largely restrained, and a desirable nanoscale domain is formed in the H6P1/PDI blend. The effect of the triphenylene pendant on the molecular alignment of the PDI molecules were also investigated by XRD (Figure S10). The introduction of PDI into the P3HT film with a weight ratio of 3:1 leads to a broad diffraction peak between 3.70–5.51°, where a sharp diffraction

dx.doi.org/10.1021/am402031v | ACS Appl. Mater. Interfaces 2013, 5, 8321–8328

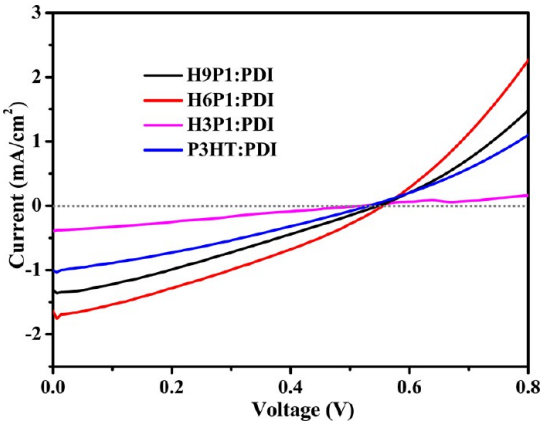

Figure 10. *J*–V characteristics of photovoltaic cells based on H9P1/PDI, H6P1/PDI, and H3P1/PDI (1:3 w/w), with P3HT/PDI (1:1 w/w) as a reference.

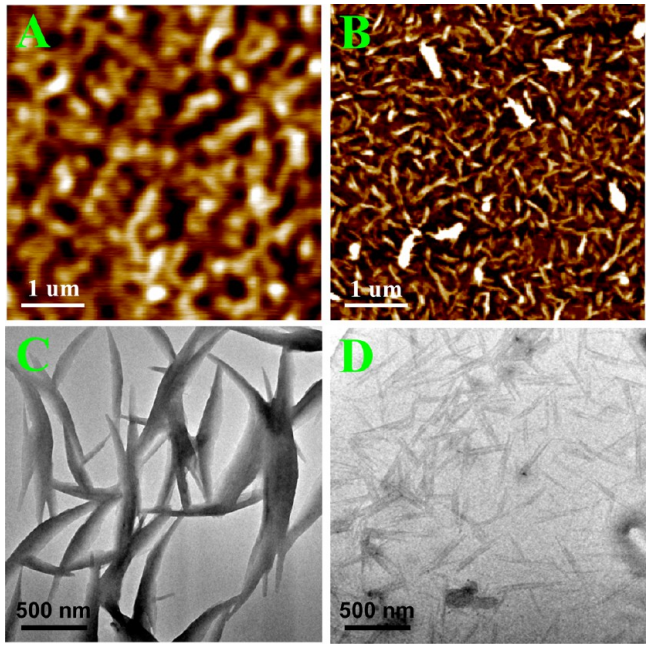

Figure 11. AFM and TEM images of the (a, c) P3HT/PDI (1:3 w/w) and (b, d) H6P1/PDI (1:3 w/w) blend films with SA + TA treatment.

peak at 4.20° is attributed to the PDI and a notable peak at 5.28° is ascribed to P3HT.[43] This suggests that there is a large phase separation induced by the crystallization of the P3HT polymer and PDI molecule, which is consistent with the morphologies observed by the AFM and TEM images. However, the introduction of PDI into the H6P1 thin film results in the appearance of a new sharp diffraction peak at 4.81° with *d*-spacing of 18.4 Å to replace the two independent diffraction peaks of PDI and P3HT, indicating the interaction between the PDI molecules and the pendant triphenylene moieties in P3HT-b-P3TPT. Thus, the cooperative assembly of P3HT-b-P3TPT and PDI provides the nanometer-scale morphology with a large interfacial surface area for efficient charge separation, which should be responsible for the enhanced J_{SC} and efficiency.

CONCLUSIONS

In this work, we have presented the synthesis of diblock copolymers (P3HT-b-P3TPT) bearing pendant triphenylene moieties by Grignard metathesis polymerization. The P3HT/P3TPT block ratios and annealing effects on the supramolecular packing behavior and optical properties of the P3HT-b-P3TPT block copolymers have been systematically investigated. Direct TA treatment develops only a disordered morphology without long-range order, whereas the SA + TA treatment can induce these block copolymers to self-assemble into highly ordered structures with lamellar nanowires. Both the well-structured organization of the diblock copolymers under slow film growth (SA) and the mesogen orientation under TA treatment are responsible for the controllable nanostructure morphology. These block copolymers are then used in BHJ solar cells with $PC_{61}BM$ or PDI electron acceptors. In the P3HT-b-P3TPT/$PC_{61}BM$ systems, the best PCE value of 1.54% was achieved using the H9P1/$PC_{61}BM$ (1:2 w/w) blend under SA + TA treatment. The lower efficiency of the P3HT-b-P3TPT/$PC_{61}BM$ device compared to that of the P3HT/$PC_{61}BM$ device is mainly because of the large-scale phase separation between P3HT-b-P3TPT and $PC_{61}BM$. Intriguingly, when the H6P1 copolymer is blended with the PDI electron acceptor, the solar cell shows a higher efficiency (0.30%) than that of the P3HT device (0.16%). The improved efficiency results from the interaction between the triphenylene moieties and PDI molecules, favoring an optimized morphology of the active layer. Therefore, the introduction of DLCs into the side chains of diblock copolymers is a highly interesting and promising design principle for novel optoelectronic materials.

ASSOCIATED CONTENT

Supporting Information

Details on the materials used, device fabrication and characterization, and methods for the NMR, thermal annealing, and solvent annealing. Synthesis of 3,6,7,10,11-pentakis(hexyloxy)-2-methoxytriphenylene (**2**), 3,6,7,10,11-pentakis(hexyloxy)-2-hydroxytriphenylene (**3**), 3-(10-bromodecyl)thiophene (**4**), 2,5-dibromo-3-(10-bromodecyl)thiophene (3BrDT) (**5**), poly(3-hexylthiophene) (**6**) (P3HT), poly(3-hexylthiophene)-b-poly-(3-(10-bromodecyl)thiophene) (**7**), poly(3-hexylthiophene)-block-poly[3-(10-(2,3,6,7,10-pentakis(hexy -loxy)-triphenyl)decyloxy)thiophene] (P3HT-b-P3TPT), and *N*,*N*′-di(2-ethylhexyl)perylene-3,4,9,10-tetracarboxylbisimide (PDI). ^{1}H and ^{13}C NMR spectra of TP, H9P1, H6P1, H3P1, and PDI. DSC thermogram of copolymers H3P1 and H6P1. Topographic images of films with different treatments. This material is available free of charge via the Internet at http://pubs.acs.org.

AUTHOR INFORMATION

Corresponding Author

*Tel: +86 791 83969562; Fax: +86 791 83969561; E-mail: ywchen@ncu.edu.cn.

Notes

The authors declare no competing financial interest.

ACKNOWLEDGMENTS

This work was supported by the National Natural Science Foundation of China (51273088 and 51263016).

REFERENCES

(1) Barrau, S.; Andersson, V.; Zhang, F. L.; Masich, S.; Bijleveld, J.; Andersson, M. R.; Inganas, O. *Macromolecules* **2009**, *42*, 4646−4650.
(2) Blom, P. W. M.; Mihailetchi, V. D.; Koster, L. J. A.; Markov, D. E. *Adv. Mater.* **2007**, *19*, 1551−1566.
(3) Muccini, M. *Nat. Mater.* **2006**, *5*, 605−613.
(4) Zhang, Y.; Tajima, K.; Hashimoto, K. *Macromolecules* **2009**, *42*, 7008−7015.
(5) Forrest, S. R. *MRS Bull.* **2005**, *30*, 28−32.
(6) Kim, H. C.; Park, S. M.; Hinsberg, W. D. *Chem. Rev.* **2010**, *110*, 146−177.
(7) Choi, S. Y.; Lee, J. U.; Lee, J. W.; Lee, S.; Song, Y. J.; Jo, W. H.; Kim, S. H. *Macromolecules* **2011**, *44*, 1771−1774.
(8) Park, S.; Lee, D. H.; Russell, T. P. *Adv. Mater.* **2010**, *22*, 1882−1884.
(9) Hong, S. W.; Gu, X.; Huh, J.; Xiao, S.; Russell, T. P. *ACS Nano* **2011**, *5*, 2855−2860.
(10) Gu, W.; Hong, S. W.; Russell, T. P. *ACS Nano* **2012**, *6*, 10250−10257.
(11) Sommer, M.; Lindner, S. M.; Thelakkat, M. *Adv. Funct. Mater.* **2007**, *17*, 1493−1500.
(12) Sommer, M.; Huttner, S.; Wunder, S.; Thelakkat, M. *Adv. Mater.* **2008**, *20*, 2523−2527.
(13) Higashihara, T.; Ohshimizu, K.; Hirao, A.; Ueday, M. *Macromolecules* **2008**, *41*, 9505−9507.
(14) Peet, J.; Heeger, A. J.; Bazan, G. C. *Acc. Chem. Res.* **2009**, *42*, 1700−1708.
(15) Tada, A.; Geng, Y.; Wei, Q.; Hashimoto, K.; Tajima, K. *Nat. Mater.* **2011**, *10*, 450−455.
(16) Ma, W. L.; Yang, C. Y.; Gong, X.; Lee, K.; Heeger, A. J. *Adv. Funct. Mater.* **2005**, *15*, 1617−1622.
(17) Mihailetchi, V. D.; Xie, H. X.; de Boer, B.; Koster, L. J. A.; Blom, P. W. M. *Adv. Funct. Mater.* **2006**, *16*, 699−708.
(18) Li, G.; Shrotriya, V.; Huang, J. S.; Yao, Y.; Moriarty, T.; Emery, K.; Yang, Y. *Nat. Mater.* **2005**, *4*, 864−868.
(19) Tang, H. W.; Lu, G. H.; Li, L. G.; Li, J.; Wang, Y. Z.; Yang, X. N. *J. Mater. Chem.* **2010**, *20*, 683−688.
(20) Chen, F. C.; Ko, C. J.; Wu, J. L.; Chen, W. C. *Sol. Energy Mater. Sol. Cells* **2010**, *94*, 2426−2430.
(21) Shrotriya, V.; Yao, Y.; Li, G.; Yang, Y. *Appl. Phys. Lett.* **2006**, *89*, 063505−063508.
(22) Peet, J.; Senatore, M. L.; Heeger, A. J.; Bazan, G. C. *Adv. Mater.* **2009**, *21*, 1521−1527.
(23) Craley, C. R.; Zhang, R.; Kowalewski, T.; McCullough, R. D.; Stefan, M. C. *Macromol. Rapid Commun.* **2009**, *30*, 11−16.
(24) Sauvé, G.; McCullough, R. D. *Adv. Mater.* **2007**, *19*, 1822−1825.
(25) Iovu, M. C.; Craley, C. R.; Jeffries-EL, M.; Krankowski, A. B.; Zhang, R.; Kowalewski, T.; McCullough, R. D. *Macromolecules* **2007**, *40*, 4733−4735.
(26) Scherf, U.; Gutacker, A.; Koenen, N. *Acc. Chem. Res.* **2008**, *41*, 1086−1097.
(27) Sergeyev, S.; Pisula, W.; Geerts, Y. H. *Chem. Soc. Rev.* **2007**, *36*, 1902−1929.
(28) Lee, J. H.; Kim, H. S.; Pate, B. D.; Choi, S. M. *Physica B* **2006**, *798*, 385−386.
(29) Schulte, J. L.; Laschat, S.; Vill, V.; Nishikawa, E.; Finkelmann, H.; Nimtz, M. *Eur. J. Org. Chem.* **1998**, 2499−2506.
(30) Hammer, B. A. G.; Bokel, F. A.; Hayward, R. C.; Emrick, T. *Chem. Mater.* **2011**, *23*, 4250−4256.
(31) Zhao, K. Q.; Chen, C.; Monobe, H.; Hu, P.; Wang, B. Q.; Shimizu, Y. *Chem. Commun.* **2011**, *47*, 6290−6292.
(32) Yu, Z. Q.; Lam, J. W. Y.; Qing, K.; Zhu, C. Z.; Yang, S.; Lin, J. S.; Li, B. S.; Liu, J. H.; Chen, E. Q.; Tang, B. Z. *Polym. Chem.* **2013**, *4*, 996−1005.
(33) Zhao, B. M.; Liu, B.; Png, R. Q.; Zhang, K.; Lim, K. A.; Luo, J.; Shao, J. J.; Ho, P. K. H.; Chi, C. Y.; Wu, J. S. *Chem. Mater.* **2010**, *22*, 435−449.
(34) Yu, X.; Xiao, K.; Chen, J.; Lavrik, N. V.; Hong, K.; Sumpter, B. G.; Geohegan, D. B. *ACS Nano* **2011**, *5*, 3559−3567.
(35) Tahar-Djebbar, I.; Nekelson, F.; Heinrich, B.; Donnio, B.; Guillon, D.; Kreher, D.; Mathevet, F.; Attias, A. *Chem. Mater.* **2011**, *23*, 4653−4656.
(36) Chen, T. A.; Wu, X. M.; Rieke, R. D. *J. Am. Chem. Soc.* **1995**, *117*, 233−244.
(37) Kline, R. J.; McGehee, M. D.; Toney, M. F. *Nat. Mater.* **2006**, *5*, 222−228.
(38) Erb, T.; Zhokhavets, U.; Gobsch, G.; Raleva, S.; Stühn, B.; Schilinsky, P.; Waldauf, C.; Brabec, C. J. *Adv. Funct. Mater.* **2005**, *15*, 1193−1196.
(39) Dittmer, J. J.; Lazzaroni, R.; Leclere, P.; Moretti, P.; Granström, M.; Petritsch, K.; Marseglia, E. A.; Friend, R. H.; Bredas, J. L.; Rost, H.; Holmes, A. B. *Sol. Energy Mater. Sol. Cells* **2000**, *61*, 53−61.
(40) Li, J.; Dierschke, F.; Wu, J.; Grimsdale, A. C.; Müllen, K. *J. Mater. Chem.* **2006**, *16*, 96−100.
(41) Rajaram, S.; Armstrong, P. B.; Kim, B. J.; Frechet, J. M. J. *Chem. Mater.* **2009**, *21*, 1775−1777.
(42) Foster, S.; Finlayson, C. E.; Keivanidis, P. E.; Huang, Y.-S.; Hwang, I.; Friend, R. H.; Otten, M. B. J.; Lu, L.-P.; Schwartz, E.; Nolte, R. J. M.; Rowan, A. E. *Macromolecules* **2009**, *42*, 2023−2030.
(43) Kozycz, L. M.; Gao, D.; Hollinger, J.; Seferos, D. S. *Macromolecules* **2012**, *45*, 5823−5832.